Post print version of "Microstructures and Mechanical Properties of $Cu/Ti_3SiC_2/C$/Graphene Nanocomposites Prepared by Vacuum Hot-pressing Sintering and Hot Isostatic Pressing"

Published in Composites Part B, 2018

Research Article

Microstructures and Mechanical Properties of $Cu/Ti_3SiC_2/C$/Graphene Nanocomposites Prepared by Vacuum Hot-pressing Sintering and Hot Isostatic Pressing

Xiaosong Jiang[1], Wanxia Liu[1], Yanjun Li[2], Zhenyi Shao[1], Zhiping Luo[3], Degui Zhu[1], Minhao Zhu[1,*]

[1]*School of Materials Science and Engineering, Southwest Jiaotong University, Chengdu Sichuan 610031, China*

[2]*Department of Materials Science and Engineering, Norwegian University of Science and Technology, Trondheim 7491, Norway*

[3]*Department of Chemistry and Physics, Fayetteville State University, Fayetteville, NC 28301, USA*

[*]Corresponding author at: School of Materials Science and Engineering, Southwest Jiaotong University, Chengdu Sichuan 610031, China. Tel: +86 28 87600715; fax: +86 28 87600723.

E-mail address: zhuminhao@home.swjtu.edu.cn (M.H. Zhu).

Abstract: Copper-graphite composite is an ideal friction material due to its good heat resistance, wear resistance and friction coefficient stability. The addition of Ti_3SiC_2 can improve strength, hardness and wear resistance of copper-graphite alloy material without affecting its self-lubricating properties and electrical conductivity. Two-dimensional graphene has become an attractive composite reinforcement owing to their unique electrical, mechanical and thermal properties. Cu/Ti_3SiC_2/C/Graphene naocomposite materials reinforced with graphene have been fabricated by vacuum hot-pressing sintering and hot isostatic pressing. Microstructures and mechanical properties of Cu/Ti_3SiC_2/C/Graphene naocomposite materials with different graphene contents have been systematically investigated. Microstructures of the composites were examined by optical microscopy, X-ray diffraction, back scattered electron imaging, scanning electron microscope with energy dispersive spectrometer and transmission electron microscope. The mechanical properties were determined from Brinell hardness, tensile, compressive and shear tests. Results demonstrated that there was an optimum value of graphene content which has an impact on microstructures and mechanical properties of Cu/Ti_3SiC_2/C/Graphene naocomposite materials. Based on graphene content on microstructure and mechanical properties of Cu/Ti_3SiC_2/C/Graphene naocomposite materials, strengthening and fracture mechanisms by graphene reinforcement have been analyzed.

Key words: Cu/Ti_3SiC_2/C/Graphene naocomposite, Vacuum hot-pressing sintering, Hot isostatic pressing, Microstructure, Mechanical properties

1. Introduction

Copper matrix graphite composites are widely used in friction materials because of the excellent electrical conductivity and thermal conductivity of copper and superior anti-friction, anti-welding, and lubrication properties of graphite [1–3].Ti_3SiC_2 has emerged as a type of material combining structure, conductivity, and self-lubrication. It exhibits properties similar to those of metal materials--high electrical conductivity, heat conduction, and ease in processing. In addition, Ti_3SiC_2 exhibits qualities similar to those of ceramics--light weight, oxidation resistance, and high temperature resistance [4–6]. Apart from the self-lubricating property and electrical conductivity of copper graphite alloy, the strength, hardness, and wear resistance of a material can be improved with Ti_3SiC_2 [4–6].The two-dimensional graphene has become an attractive composite reinforcement because of its distinct electrical, mechanical, and thermal properties [7–13]. Most studies on copper matrix composites have thus far focused on single reinforcements [14–15]. However, the enhancement effect of single reinforcements cannot meet the requirements for its application, whereas the comprehensive functions of two or multiple reinforcements can be considered [16–17]. Ti_3SiC_2 and graphene can be regarded as two types of reinforcement, given that Ti_3SiC_2 possesses properties of both metal and ceramic. Graphene is recognized for its strength at the nanoscale level. Adding graphene to the Cu–C matrix may produce synergistic, cooperative, and multi-scale reinforcements [4–13,16–17]. The choice of reinforcement and design significantly influences the performance of the composite. Several studies have been conducted on the preparation of graphene-reinforced copper matrix composites. Chemical vapor deposition, hot isothermal pressing, and spark plasma sintering can be used to prepare copper matrix composites, which can determine the microstructures and properties of materials [18–20].

On the basis of the preparation method of graphene-reinforced copper matrix composites, the interface mechanism between nanocarbon materials and metal matrix has drawn increased interest, which can help elucidate the basic mechanical properties of composites to provide a theoretical basis for the design of graphene-reinforced copper matrix composites. An interface reaction occurs between multi-walled carbon nanotubes (MWCNTs) and aluminum, which can lead to Al_4C_3 generation [21–22]. According to density functional theory, active adsorption sites exist between Cu and MWCNTs, particularly on top of the carbon atom on the outer wall of MWCNTs. Theoretically, Cu and MWCNTs can be bonded under certain conditions [23–25]. The interaction between graphene and metal matrix has also attracted the attention of many researchers [26–30]. The dynamic exfoliation of graphene on the crystal surface of Cu was examined based on molecular dynamics, and the results show that graphene has the highest surface binding energy in the Cu(111) direction[31].The elastic properties and deformation mechanisms of graphene and Cu nanocomposites were investigated by Giannopoulos[32]. The theoretical analysis provides the possibility of designing a better interface between graphene and Cu[33–34].The surface of graphene is smooth and has a conjugated bond structure, which exhibits high chemical inertness and hydrophobic properties [35–36].The surface energy of graphene is high, facilitating stacking and gathering as aggregation occurs frequently in metal matrix composites[26–30,37].This

property impedes the formation of an interface between graphene and Cu to hinder the performance of graphene [26–30,37]. Accordingly, the composite interface and a new method of graphene surface treatment need to be further investigated between graphene and Cu.

At present, numerous studies have been conducted on graphene-reinforced polymers in which the theoretical system and the preparation process are relatively perfect [38–42]. However, graphene-reinforced copper matrix composites are presented with many challenges, which are attributed to the difficulty of graphene dispersion without damaging the structure of graphene, poorer interfacial bonding between graphene and copper, high-density preparation. Thus, high-performance graphene-reinforced copper matrix composites are difficult to obtain [43]. In addition, the relatively low density of these composites becomes an obstacle in its application [19–20,37]. In the present study, surface modification of graphene was conducted to improve its dispersion, and Ti_3SiC_2 particles were added to the Cu–C matrix to obtain multiple phases. Cu/Ti_3SiC_2/C/Graphene nanocomposites were prepared from raw materials of graphene, graphite, Ti_3SiC_2 and electrolytic copper powder by vacuum hot-pressing (VHP) and hot isostatic pressing (HIP). To evaluate the effect of graphene on the properties of Cu matrix composites, Cu/Ti_3SiC_2/C/graphene nanocomposites with graphene contents equal to 0.5 wt.%, 1 wt.%, and 1.5 wt.% were prepared. Microstructural observation and mechanical property testing of Cu/Ti_3SiC_2/C/graphene nanocomposites were conducted to evaluate the reinforcing effects**.** Strengthening and fracture mechanisms of Cu/Ti_3SiC_2/C/graphene nanocomposites were discussed on the basis of the experimental results.

2. Experimental Procedures

Cu/Ti_3SiC_2/C/Graphene nanocomposite materials were designed based on the concept of multi-phase composites and prepared by powder metallurgy re-pressing methods—that is, VHP sintering and HIP. The process includes mechanical ball-milling, compacting, and sintering process in which a component is subjected to both elevated temperature and high pressure [44].The physical parameters of graphene, graphite powder, Ti_3SiC_2 powder, and electrolytic copper powder used as raw material are listed in Table 1. Dispersions of graphene assisted by ultrasonic oscillation, plasma, and chemical treatment surface modification were prepared using Ar-NH_3 plasma and 0.02μg/mL rutin solution[45–46].The raw powders consisting of 10 wt.% Ti_3SiC_2, 3 wt.% graphite, different contents of graphene (0.5 wt.%, 1.0 wt.%, 1.5 wt.%) and copper were mixed by high-energy ball milling for 1 h. Composite powders were heated from room temperature to 950°C and applied with pressure of 27.7 MPa for 30min. After pressure was unloaded, the powders were kept warm for 2h and then cooled inside the furnace to room temperature. The samples obtained by hot pressing were treated by HIP. The temperature increased from room temperature to 650°C with 0.6 MPa pressure, and warming compression was kept at 950°C and 100 MPa for 2h.The relative densities of nanocomposite materials were analyzed by measuring the apparent density of the drainage material on the basis of Archimedes' principle. Microstructures of Cu/Ti_3SiC_2/C/graphene nanocomposite materials were characterized by optical microscopy (OM,

AxioCam MRC5), X-ray diffraction (XRD, X'Pert Pro-MPD), scanning electron microscopy (SEM, JEOL JSM-7001F at 15 kV) with back-scattered electron (BSE) imaging mode and energy dispersive X-ray spectrometry (EDS), and transmission electron microscopy (TEM, FEI Tecnai F20ST at 200 kV). Hardness measurement was conducted using a Vickers hardness tester (HV, HXD-1000TM). Tensile, compression, and shearing testing were performed using a microcomputer-controlled electronic universal testing machine (WDW-3100) at a loading speed of 0.5 mm/min.

TABLE 1:Properties of the raw material powders.

Material	Density(g/cm^3)	Size	Purity(%)
Graphene	2.1	≤5 Layers	≥99.8
Ti_3SiC_2	4.53	200 Mesh	
C	2.2	250 Mesh	
Cu	8.89	300 Mesh	≥99.99

3. Results and discussion

3.1 Characterization of nanocomposite powders

The SEM images of the mixture of graphene, graphite powder, Ti_3SiC_2 powder, and electrolytic copper powder after ball milling are presented in Figure 1.As shown in Figure1a, copper particle clusters are subjected to cold welding by diffusion produced during high-pressure ball-milling. In Figures 1a and 1b, a transparent laminar structure of graphene can be observed adhering or embedding in the copper particle clusters that the ball-milling process can promote the interfacial bonding between the matrix and the reinforcing phase [47]. The reinforcing phase contains some fragments as a result of the mechanical action of ball-milling, which reduces the size of the reinforcing phase to a certain extent and contributes to the homogeneous dispersion of the reinforcing phase, as shown in Figure1d. Ball-milling can change the shape of powder particles. Rounder particles indicate poorer effect of ball-milling and cold-welding [48]. In the current study, cold-welding between copper particles is significant, and a small amount of graphene adheres to the copper particles. This occurrence indicates satisfactory overall mixing effect and that the addition of graphene does not affect the structural characteristics of the overall material.

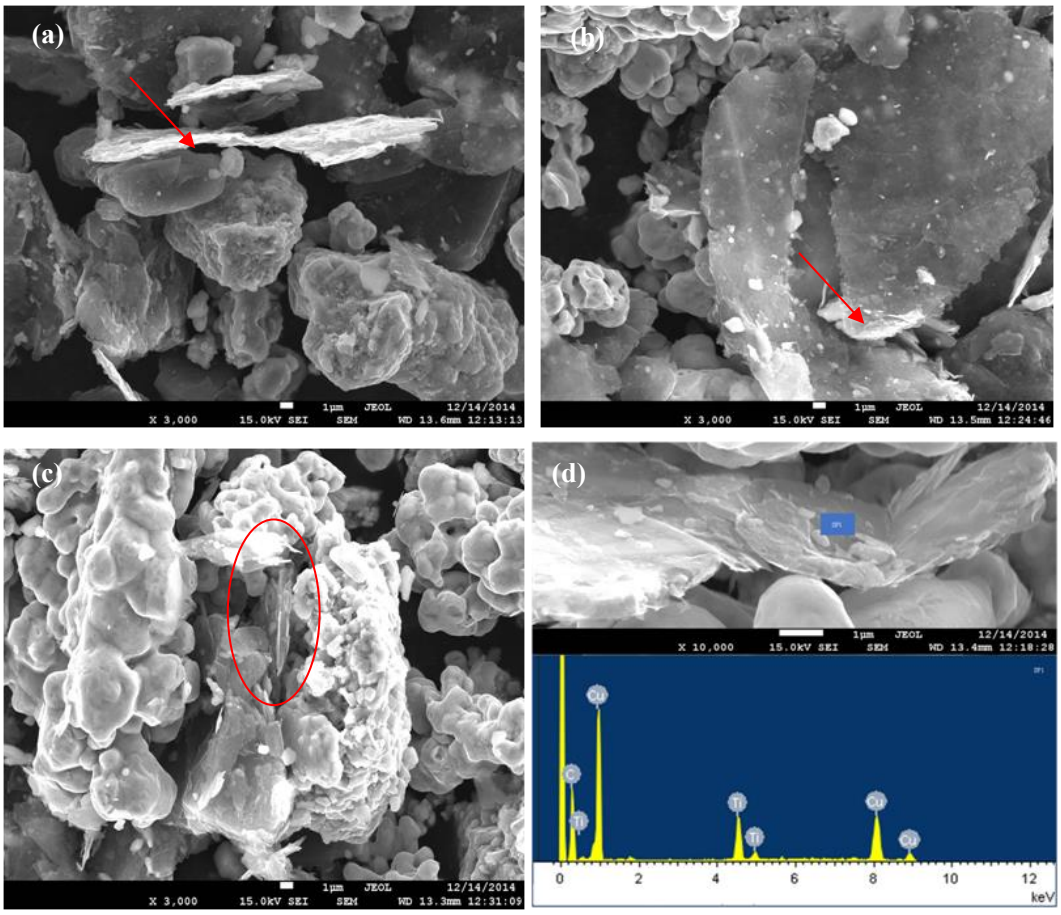

FIGURE 1: (a-c) SEM images of raw materials of graphene, graphite powder, Ti_3SiC_2 powder and electrolytic copper powder after ball milling; (d) EDS from Fig.1(d).

3.2 Microstructure and phase identification of nanocomposite materials

With an increase in graphene content, the compactness of the copper matrix composite is decline, as revealed in Table 2. When graphene content is 0.5 wt.%, the composite achieves the highest compactness of 98.17%. When graphene content is increased to 1.0 wt.%, compactness decreases to 96.85%, indicating that graphene content affects the compactness of the composite. During the sintering process of copper graphite powder metallurgy composite materials, the copper phases in a semi molten state connect to each other to reduce the surface energy so that it can increase the sintering neck area and resulting in agglomeration graphene or graphite retained in the gap. Due to the large surface area and high surface energy of graphene, it will absorb more easily nucleated substances during nucleation cooling in order to reduce the total free energy. Moreover, owing to the small size of graphene, it will reduce nucleation energy and improve nucleation rate. However, graphene aggregation do not play a role in grain refinement because it will grow up to hinder the sintering and sintering neck bonding between copper particles. Therefore, when graphene content is increased, the presence of Van der Waals' forces and large π bonds facilitates aggregation, impedes the

sintering process of the copper matrix (i.e., formation of a sintering neck), increases the number of voids, and increases porosity.

TABLE 2: Relative densities of naocomposite materials

Graphene(wt.%)	Theory density(g/cm^3)	Actual density(g/cm^3)	Relative density (%)
0.5	7.43	7.29	98.17
1.0	7.34	7.11	96.85
1.5	7.25	7.04	97.11

VHP sintering is the process of Cu/Ti_3SiC_2/C/graphene nanocomposite densification, which is mainly divided into three stages: contact of particles with one another, neck formation caused by a shaping flow and grain boundary slip, and grain boundary diffusion. The existence of graphene can prevent the abnormal growth of copper matrix [49]. However, VHP sintering fails to completely close the gap. HIP treatment is needed to compact nanocomposites, which can achieve complete densification and homogenization between direction parallel and perpendicular to pressure direction. Figures 2(a) and 2(b) illustrate the change in shape of copper particles by VHP sintering in which direction I is parallel to the pressure and direction II is perpendicular to the pressure. Figures 2(c) and 2(d) are metallographic results of sintered nanocomposites. As shown in Figure 2(c), the black reinforcement phase is mostly embedded in the copper particles, and the black enhancement phase in Figure 2(d) is the strip distribution along the copper grain boundary. The electrolytic copper powders used in the current study are uniform in size and regular in shape and can be compressed to an oblate form after single-phase loading during VHP sintering [44]. The diameter of the copper particles in direction I is smaller than that in direction II. Reinforcements can be dispersed along the copper surfacein direction II, in which it is linearly distributed along the copper grain linearly, whereas in direction I, it is an irregular block.

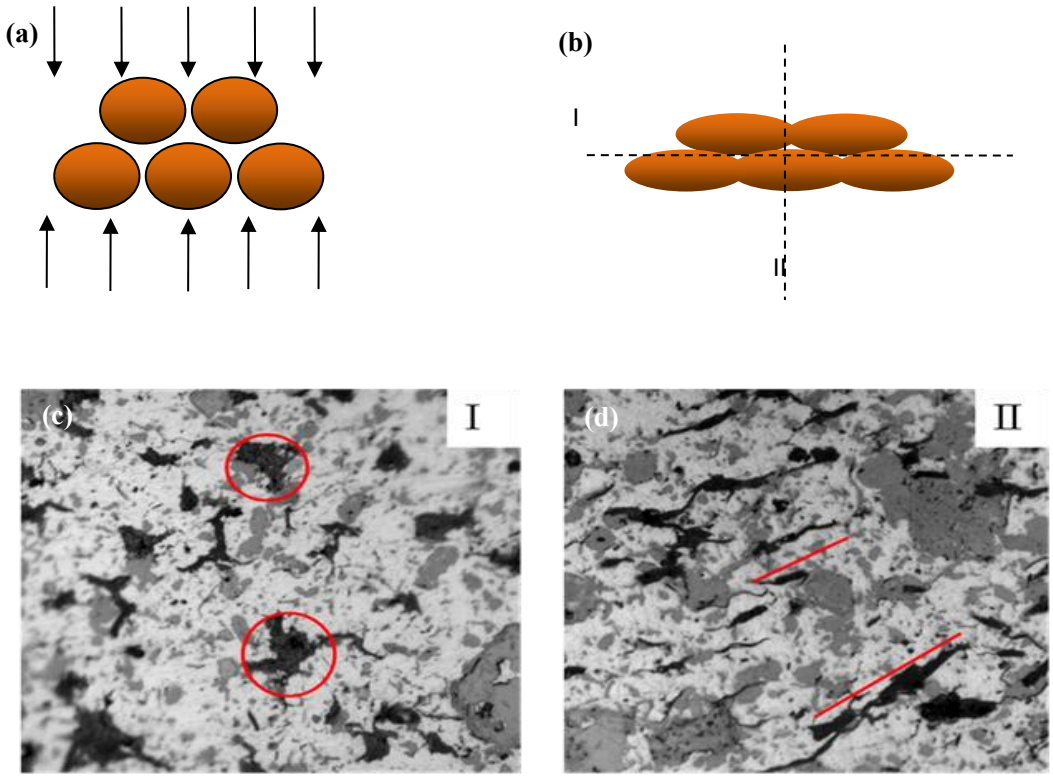

FIGURE 2:(a, b) Schematic diagram of copper particles shape change by vacuum hot-pressing sintering, in which direction I is parallel to the pressure and direction II is a perpendicular to the pressure. (c, d) Metallographic results of sintered nanocomposites.

Graphene can absorb substances prone to nucleation during copper nucleation and cooling. Addition of a small quantity of graphene, which is taken as a nanophase, can reduce nucleation energy and improve the nucleation rate. When a proper amount of graphene is added to the nanocomposite, there is no graphene aggregation and it can be completely coated by a copper matrix so that nanocomposite with excellent performance can be obtained. Graphene is filled in the pores of the nanocomposite which can increase the density and hinder the matrix fusion during pressing and sintering. With the increase of graphene content, because the size of graphene is larger than the metal lattice of copper, it is easily aggregated on the grain boundary when its content exceeds a certain value so that the continuity of the copper matrix is separated and the binding force between the crystals is weakened. Graphene is damaged to a certain extent during ball-milling. An irregular five-membered ring, seven-membered ring, and other structures can form a fulcrum [37]. Addition of graphene can refine the microstructure. On the basis of the BSE patterns of the sintered nanocomposites with different graphene contents shown in Figure 3, the microstructure of the composite containing 0.5wt.% graphene was homogeneous and tiny. Agglomeration of the reinforcing phase intensified with an increase in graphene content. White base is identified as the copper matrix, whereas the gray block is identified as

Ti_3SiC_2. The black strip consists of graphite and graphene. The number and area of the black zones increased significantly, and several large black zones were observed. These observations indicate that the agglomerated graphene plays no role in refining the grains. Agglomeration of graphene may impede the sintering and binding of copper particles and growth of sintering neck, influence material migration in copper atoms, reduce binding among copper matrices, and increase porosity. An increase in graphene content during sintering can reduce, to a certain extent, the fluidity of the semi-molten copper matrix and the homogeneity as well as exert an adverse effect on pores filling and sintering neck formation. The reinforcing phase was evenly distributed in the copper matrix, and a considerable amount of graphite was evenly distributed in the margin of titanium silicon carbon in the grey area (as shown in Figure 4), which can influence the reinforcing effect.

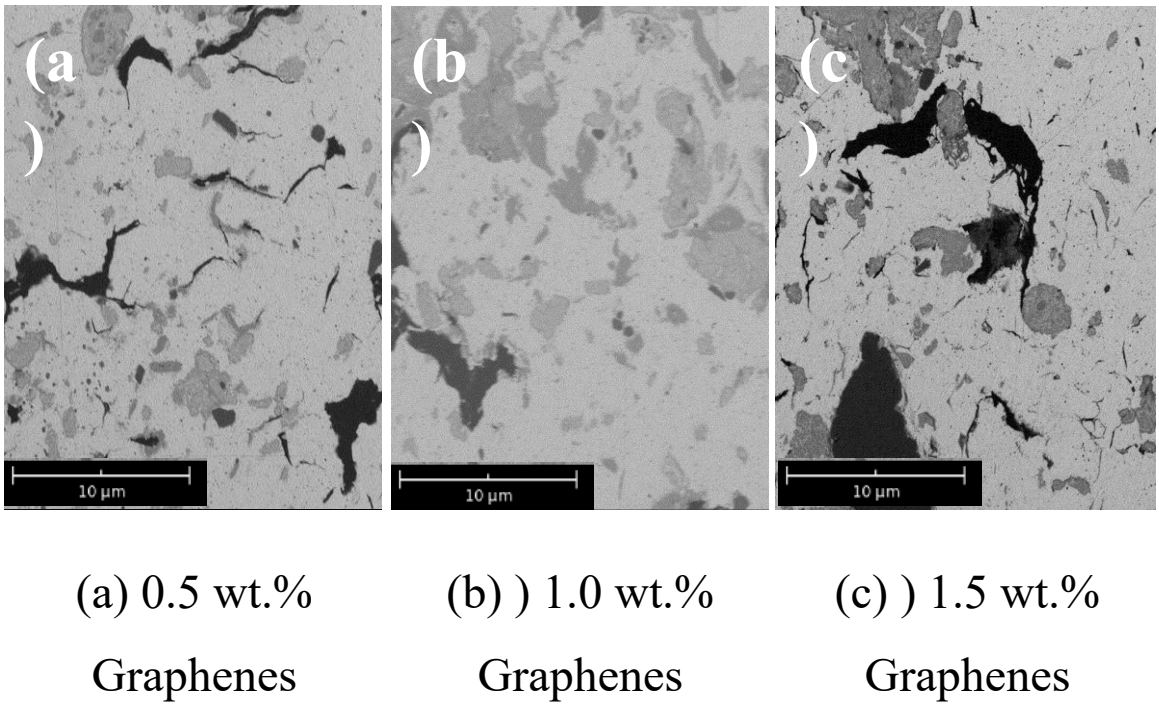

FIGURE 3: BSE patterns of sintered nanocomposites: (a) Sintered nanocomposites with 0.5 wt.% graphene, (b) Sintered nanocomposites with 1.0 wt.% graphene, (c) Sintered nanocomposites with 1.5 wt.% graphene.

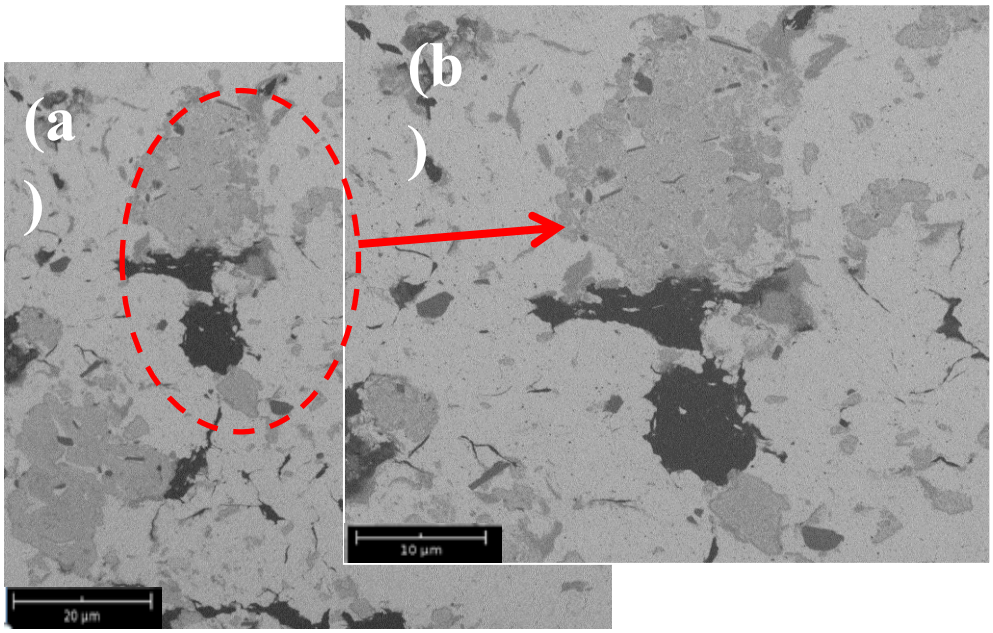

(a) 0.5 wt.% Graphenes (b) 0.5 wt.% Graphenes

FIGURE 4: BSE patterns of sintered nanocomposites with 0.5 wt.% graphene.

To further identify the products, the microstructure of the nanocomposites sintered is analyzed by SEM surface scanning. As shown in Figure5(a), all particles are evenly distributed with copper, titanium, and silicon, which is consistent with the afore mentioned BSE results in Figures 3 and 4.Figure 5 shows that the Cu, Ti, and Si are almost similarly distributed and that no gap is present between the two phases. This observation indicates that Ti_3SiC_2 and Cu matrix exhibit excellent wettability. From the SEM results of the previous analysis, the position of the distribution of Cu, Ti, and Si complemented with the distribution of graphite and graphene. This finding suggests that graphite neither wets the metallic copper nor reacts with metallic copper and that the formation of a strong interface presents a challenge.

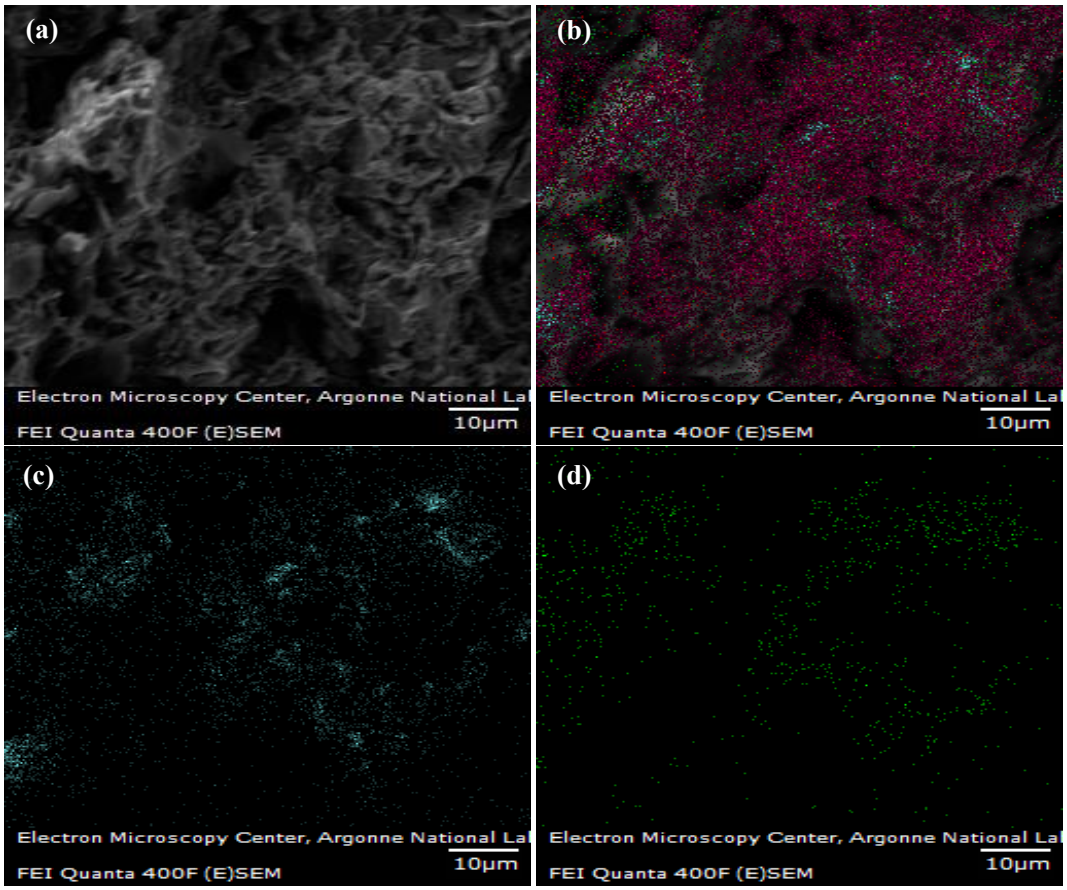

FIGURE5: SEM surface scanning analyses of sintered nanocomposites. (a) SEM; (b) Cu map; (c) Ti map; (d) Si map.

Figure 6(a) presents a dark-field TEM image of copper matrix composites with a mass fraction of 0.5 wt.% graphene. Figures 6(b–e) show the corresponding local magnifications in Figure 6(a). In contrast to the EDS diagram of sp1 and sp2 in Figure 6(b), the copper matrix in the photo appears bright and gray, and the gray Ti_3SiC_2 is embedded in Cu. Figure 6(c) is surrounded by a dashed line of Cu particles. The shortest line has a diameter of about 50nm, whereas the longest line has a diameter measuring about 200nm, compared to the beginning of raw material electrolytic copper powder 300μm reduced many. These findings indicate that the addition of a reinforcement phase played a role in strengthening the fine grain of Cu [50]. As can be observed in Figures 6(d) and 6(e), the dark-gray phase is the reinforcement phase, whereas the gray-white phase is the matrix phase. The sp3 EDS results in Figure 6(d) show that C has a high content, suggesting that graphene exists in the region. The result shown in Figure6 shows the presence of graphene at the edge of the sample.

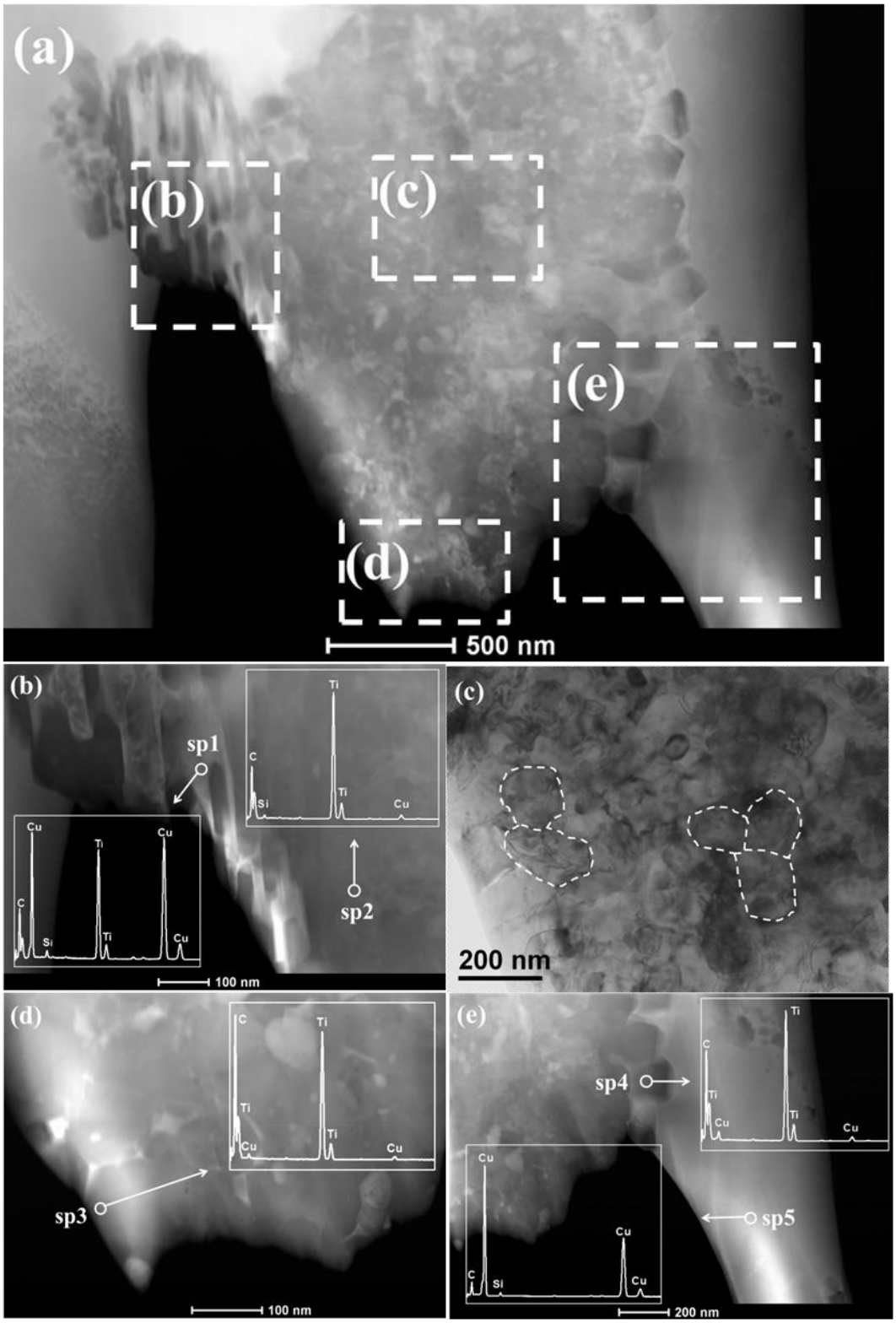

FIGURE 6: (a) TEM image of sintered nanocomposites with 0.5wt% graphene. (b, c, d, e) Magnified TEM image of local amplification corresponding to Fig. 6(a). Inserted in (b, d, e) is EDS spectra taken from the marked cross symbol spots.

Figures 7(b) and 7(c) are present diffraction photographs of TiC and Cu, respectively. Figure 7(d) shows an enlarged view of TiC in Figure 7(a).These observations indicate that Ti_3SiC_2 decomposition occurred during VHP; however, small amounts of Cu_9Si particles remained. Research indicates that the interfacial reaction between Cu and Ti_3SiC_2 was mainly attributed to the interfacial reaction between Cu and Ti_3SiC_2, and that interfacial reaction between Cu and Ti_3SiC_2 was promoted. The interfacial reaction between Cu and Ti_3SiC_2 can improve the wettability of the system in that diffusion of elements leads to the formation of a reaction intermediate, which can change the interface structure of the system to promote interfacial bonding between Cu and Ti_3SiC_2[51].

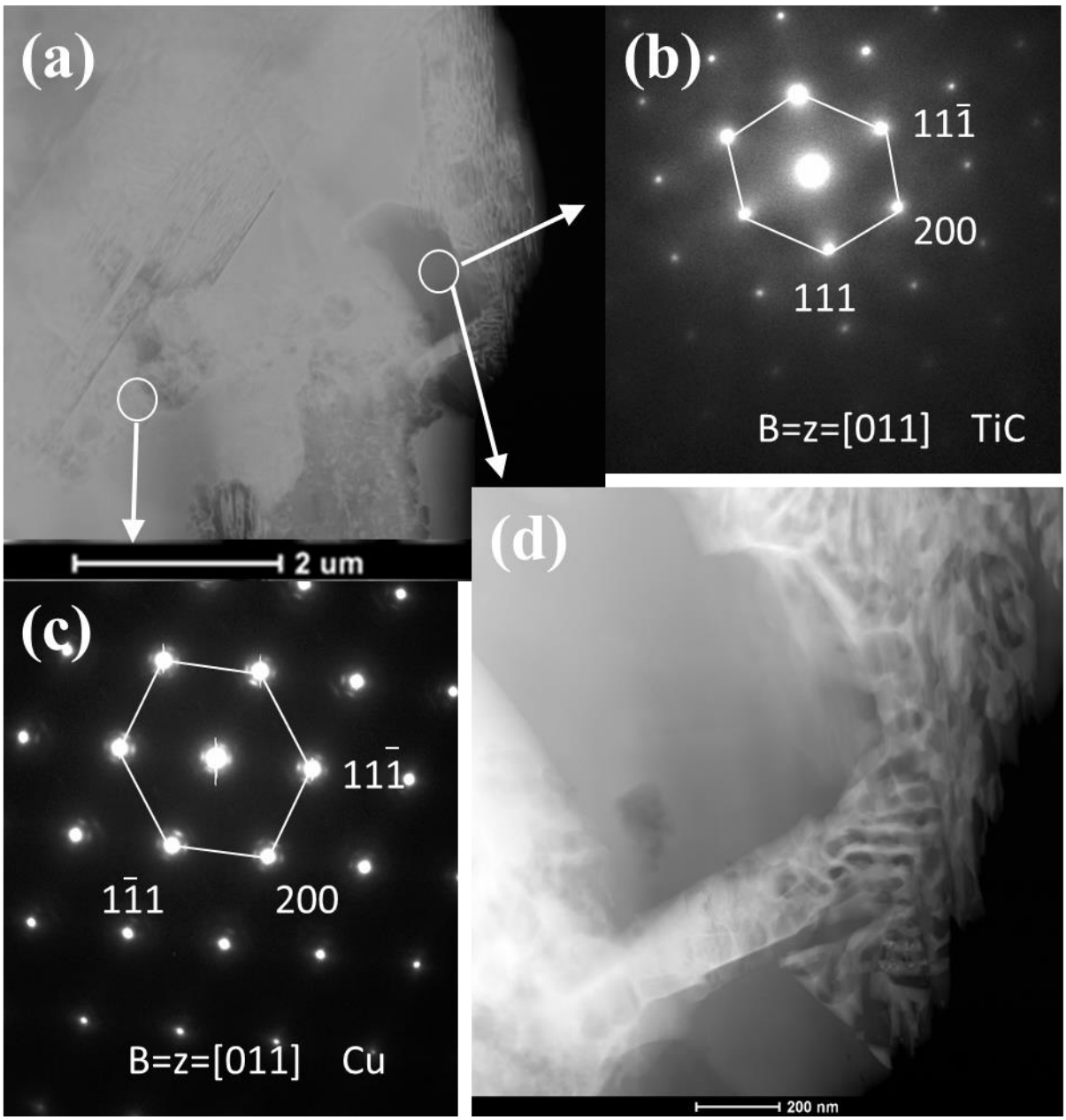

FIGURE 7: (a) TEM image of sintered nanocomposites with 0.5 wt.% graphene. (b, c) Diffraction patterns from Cu matrix and TiC. (d) Magnified TEM image of local amplification corresponding to Fig. 7(a).

Figure 8 shows the XRD patterns of the nanocomposites in which TiC and Cu_9Si were detected. The same substance was detected in three types of Cu/Ti_3SiC_2/C/graphene composites with different graphene contents, indicating that graphene content exerts no effect on the generation of TiC and Cu_9Si. That is, the thermal decomposition of Ti_3SiC_2 was not related to graphene content. Ti_3SiC_2 thermal decomposition can occur at approximately 950°C for Ti_3SiC_2 and Cu composites [16]. When the temperature exceeds 450°C, the silicon reacts with Cu, forming a Cu_9Si compound. When the composites are maintained for 2 h at a temperature lower than 950 °C, Ti_3SiC_2 is inferred to be subject to slow decomposition and generates TiC, and the reaction product of silicon reacts with copper matrix, forming Cu_9Si. The main reactions are as follows:

$$Ti_3SiC_2 = 3TiC_{2/3} + Si \quad (1)$$

$$C + Si = SiC \quad (2)$$

$$SiC + 9Cu = Cu_9Si + C \quad (3)$$

$$Si + 9Cu = Cu_9Si \quad (4)$$

Standard molar generation of Gibbs free energy change can be used to determine the direction of a chemical reaction. The standard molar generation of Gibbs free energy is expressed as

$$\Delta_r G^{\emptyset}{}_m = \sum v_b \, \Delta_f G^{\emptyset}{}_m \quad (5)$$

In this study, $\Delta_r G^{\emptyset}{}_m$ is the standard molar Gibbs free energy change of the chemical reaction; v_b is the stoichiometric number in the reaction formula, given that the product v_b is positive and the reactant v_b is negative; and $\Delta_f G^{\emptyset}{}_m$ stands for the standard molar generation of Gibbs free energy. The relationship between $\Delta_r G^{\emptyset}{}_m$ and $\Delta_f G^{\emptyset}{}_m$ of the reaction is calculated. When $\Delta_r G^{\emptyset}{}_m < 0$, the reaction can occur positively. When the Gibbs reaction free energy is 1200K, $\Delta G_{f(Ti_3SiC_2,1200K)}$ is 248.54kJ/mol, and $\Delta G_{f(Si,1200K)}$ is 39.66kJ/mol. Therefore, $\Delta_r G_m$ of Reaction (1) is -231.68 kJ/mol, which is negative, and a reaction occur. By thermodynamic calculation of Reaction (2), $\Delta_r G_m$ is -55.44kJ/mol which is also negative, so that Reaction (2) can occur. Reaction (4) is more likely to occur than Reaction (3) because (4) - (3) = (2), where $\Delta_r G_m$ of Reaction (2) is -55.44 kJ/mol. As a component of hard alloy, TiC is characterized by high melting point, high hardness, and high brittleness. Cu_9Si is also a brittle compound and an instable phase. Formation of the brittle phase is likely to cause stress concentration. However, the presence of hard reinforcement phases has endowed composites with good tribological (friction and wear) characteristics [52–55]. Therefore, the two compounds generated during the decomposition of Ti_3SiC_2 can adversely affect the properties of the copper matrix composites. The XRD results in Figure 8 shows TiC formation, and the TEM results in Figure 7 reveal the morphology of the TiC hard particles in the matrix. The results of XRD characterization are consistent with the TEM characterization.

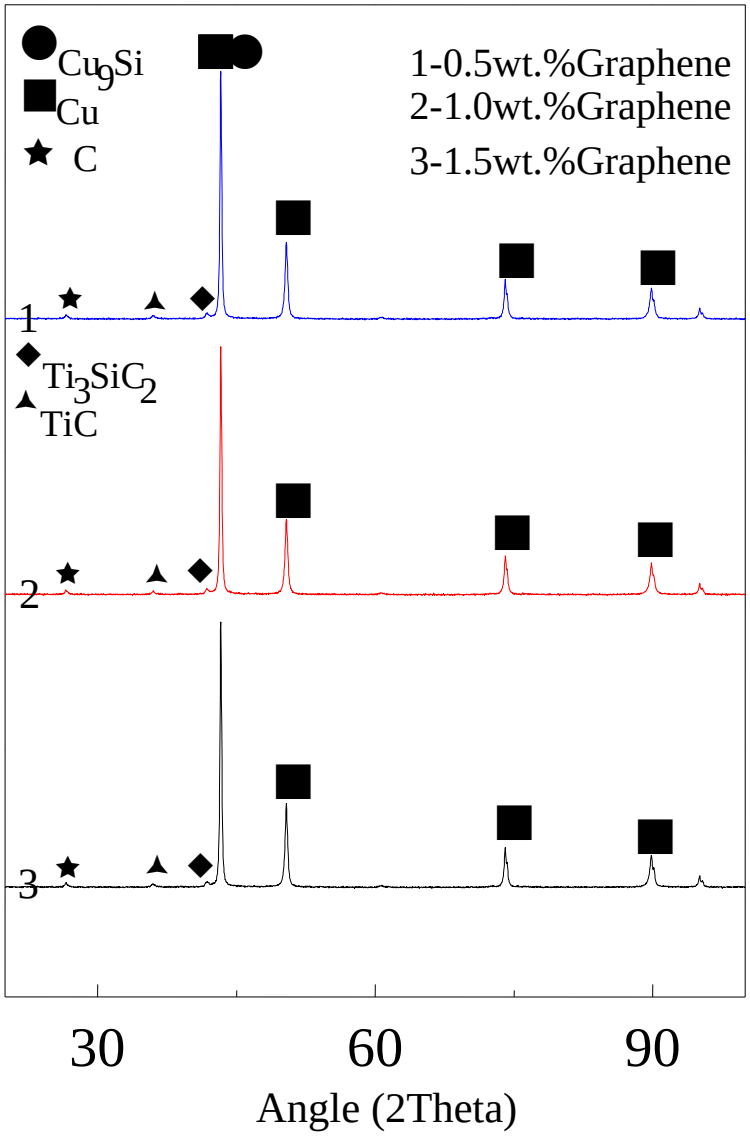

FIGURE 8: XRD patterns of sintered nanocomposites.

Figure 9 (b) shows a partial enlargement of graphene bonded to the matrix in Figure 9(a). As shown, graphene is translucent and has curled edges. Graphene is still monolayer or less in the composite. In addition, graphene is presumed to be evenly dispersed in the composites. Figures 9(c) and 9(d) present HRTEM images of the Cu matrix composites. Cu and Ti_3SiC_2 are clearly determined by measuring the interplanar spacing. Cu is exhibits good wettability with graphene and Ti_3SiC_2, which explains the uniform dispersion of the reinforcement in the matrix and the effective interface combination to ensure the high performance of composite materials.

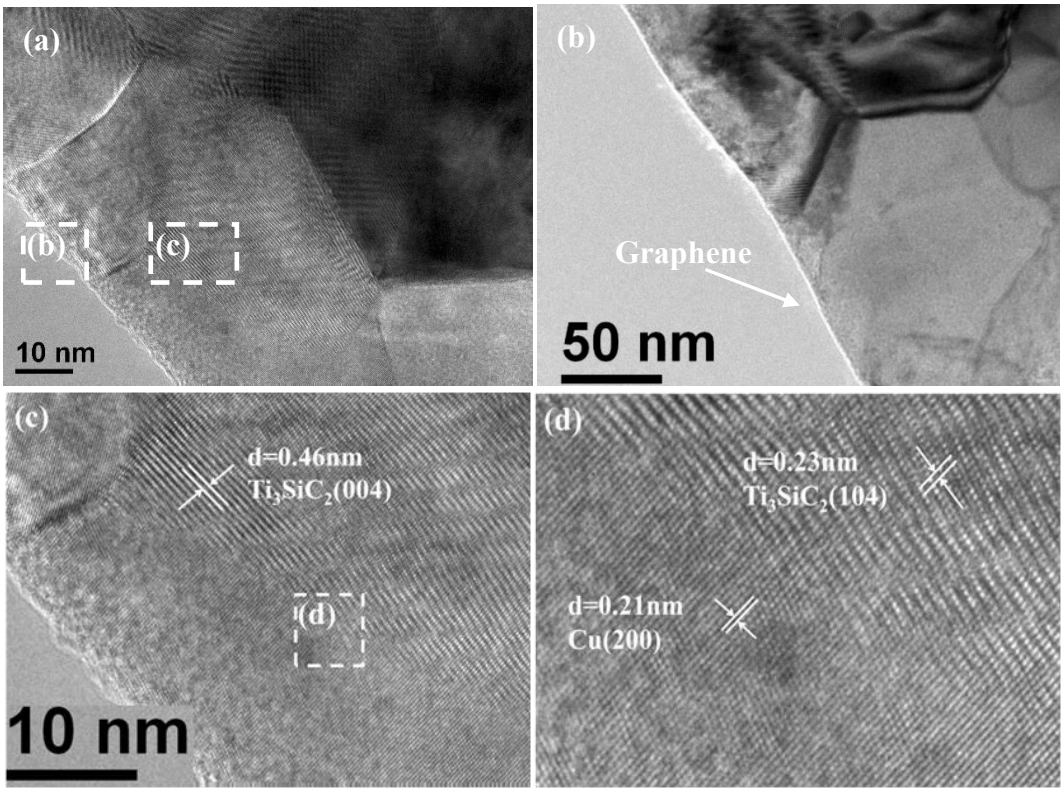

FIGURE 9: (a) TEM image of sintered nanocomposites with 0.5 wt.% graphene. (b, c) Magnified TEM image of local amplification corresponding to Fig. 9(a). (d) Magnified TEM image of local amplification corresponding to Fig.9(c).

3.3Mechanical propertiesand tensile fracture analysisof nanocomposite materials

The results of the Vickers micro-hardness test are listed in Table 3.When the mass fraction of graphene was increased to 1.5wt.% from 0.5wt.%, the hardness of graphene exhibited a decreasing trend. On the basis of the rule of mixtures, graphene can increase the hardness of the composite if the reinforcing phase is evenly distributed in the matrix. A higher mass fraction of graphene can result in higher hardness. However, in the current study, a larger quantity of graphene led to lower hardness of the composite. The main causes are as follows: (1) A series of defects, such as pores, may lead to this phenomenon. Decreased compactness can lead to increased porosity and decreased structural homogeneity. Meanwhile, the presence of pores can also reduce the elasticity modulus and hardness of the composite[56].(2) With increased graphene content, a large specific surface area of graphene and the presence of the Van der Waals' force prompted graphene to agglomerate, weakening its reinforcing role [57]. The increased reinforcing phases influence sintering, decrease interfacial bonding, and reduce the properties.

TABLE 3:Mechanical properties of sintered naocomposite materials.

Item	HV	Compressive strength (MPa)	Tensile strength (MPa)	Shear strength (MPa)
0.5 wt.%	129.17(±11.89)	467.97(±10.26)	250.92(±12.38)	129(±9.85)
1.0 wt.%	123.84(±9.56)	446.03(±4.64)	214.38(±2.70)	106(±3.32)
1.5 wt.%	121.57(±9.71)	435.26(±11.58)	174.67(±7.62)	89(±7.40)
Cu/Ti_3SiC_2/C[58]	85	/	113	/
Cu/Ti_3SiC_2/C/MWCNTs[16]	91	301.8	126.92	/

※Multi-Walled Carbon Nanotubes(MWCNTs).

The measured mechanical properties of the nanocomposites are listed in Table 3.When the soft coefficient (α) of the stress state of the single-direction compression experiment is 2, the mechanical behavior of the material exhibiting brittleness under tensile force is in the plastic state. As shown in Table 3, when the mass fraction of the graphene is 0.5 wt.%, the highest compressive strength of the composite is obtained. The compressive strength exhibits a decreasing trend, similar to the trend depicting the mechanical property. The main factors influencing the strength of the composites include porosity, interface, homogeneous dispersion of graphene, and grain size of the copper matrix [59–61]. When the graphene content was higher than 0.5wt.%, the transfer of the folded structure weakened the stress and the interfacial bonding with the copper matrix because of agglomeration. Given that the increased pores were equivalent to the sources of micro-cracks, the compressive strength of the composite declined.

The shear strength of the nanocomposites is listed in Table 3. As presented in the diagram, the highest shear strength of the composite was obtained when the graphene content was 0.5wt.%. The shear strength reflects more of the cohesive force of the material—that is, the mutual connection between the atoms and molecules of the material. Thus, the shear strength can reflect the conditions of the interfacial bonding between the copper matrix and the reinforcing phase [62]. The shear strength decreased with an increase in the graphene content. On the basis of this analysis, graphene and the copper matrix had a large contact area, given that graphene had a large specific surface area and small thickness, which effectively promoted interfacial bonding and transfer of shear strength [63]. However, when the graphene content increased, agglomeration exerted no strengthening effect on the graphene and significantly decreased the mechanical properties of the composite.

Tensile deformation curves of the nanocomposites are presented in Figure 10.The tensile strength of the composite reached its maximum when the mass fraction of graphene was 0.5wt.%. With an increase in graphene content, tensile

strength decreased. The mechanical properties of the composites were associated not only with the compactness but also with the degree of homogeneous dispersion of the reinforcing phase in the matrix and the size of the copper matrix grains [64–65]. The compactness and metallographic analysis indicates the presence of voids in the composite. The voids are equivalent to microcracks within the material. They are likely to become the sources of microcracks and can reduce the mechanical properties of the material. With an increase in graphene content, the tensile strength of the composite almost exhibited a linearly decreasing trend. The reduction in its mechanical properties could be associated with graphene agglomeration. The high strength and the reinforcing phase failed to exert their influence after graphene agglomeration; however, the graphite and graphene retained in the voids became a lubricant in subsequent frictional wear and current-carrying frictional wear. The cracks would be impeded by graphene and the path would change to extend along the graphene surface if graphene did not agglomerate and could evenly disperse. The bonding strength between graphene and the copper matrix plays an important role in improving the mechanical properties.

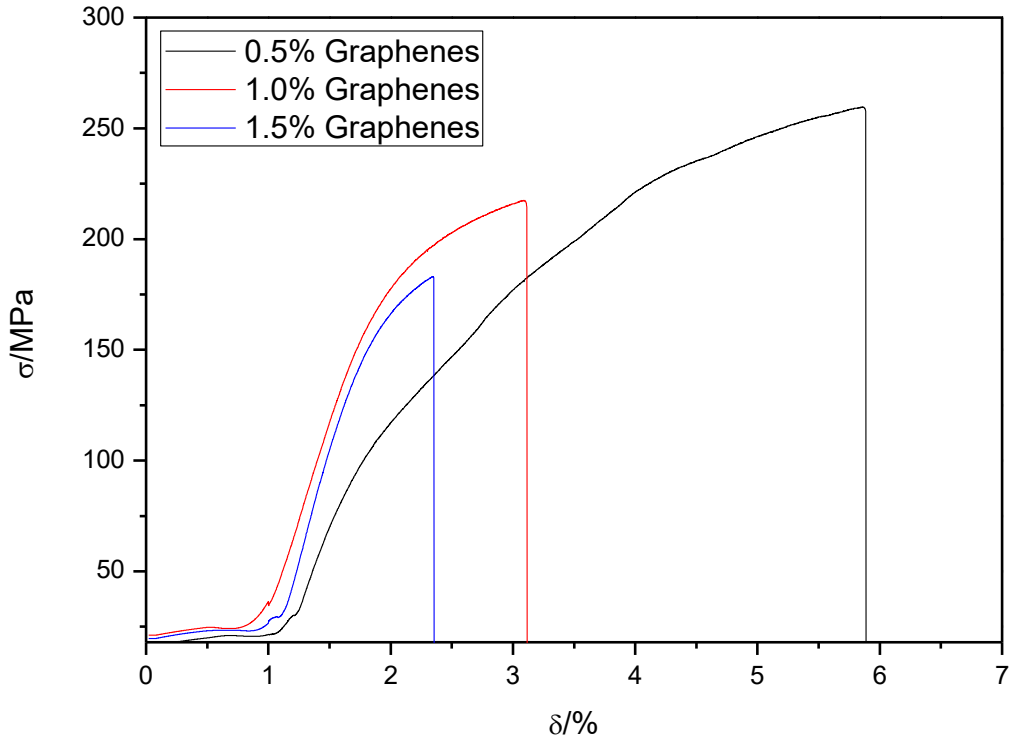

FIGURE 10: Tensile deformation curves of sintered nanocomposites

Figures 11 and 12 present the SEM analyses of the tensile fractures and a schematic of the tensile fracture microscopic process of the nanocomposites. The fractures of the nanocomposites were straight as indicated in Figure 11, which shows fracture orientation perpendicular to the maximum normal stress and dimples related to material plastic deformation. Figures 11 (a-b) and Figure 12 (a) are the SEM images of fractures of the sintered nanocomposites (0.5

wt.%, 1.5 wt.% , 1.0 wt.%) with the same magnifications (500X). The shape of the dimples can be seen clearly as it is indicated that the sintered nanocomposites has a plastic deformation during the tensile process. With the increase of graphene content, the diameter of the dimple is larger. Figures 11 (c-e) are the SEM images of typical fractures of the sintered nanocomposites (0.5 wt.%, 1.0 wt.%, 1.5 wt.%). So it is clear that a good interface is formed between graphene and copper and graphene is evenly dispersed in the matrix. Figures 11(f) is the magnified SEM image of local amplification corresponding to Fig. 11(e). When the sintered nanocomposites bear the external tensile stress, graphene also bears the load through interfacial stress transfer. Within the red circle in Figures 12(a-b) are the agglomerated graphene sheets. The graphene sheets were embedded into the copper matrix and properly bonded with the copper matrix. The graphene had a large specific surface area. The characteristic contact area helped increase the contact area between the graphene and the matrix and promote interfacial bonding with the copper matrix. Meanwhile, a properly bonded interface could impede dislocation motion [66–67]. The distance that the dislocation needed to bypass could also increase during crack propagation. The graphene layer was thin, and the gaps among the copper matrix grains were considerably small. These characteristics helped transfer the external force from the copper matrix to graphene and directly use the ultra high strength of graphene. The high strength of the material would be achieved accordingly. The graphene sheets had a unique folded structure. When force was applied on the composite, graphene underwent fold flattening and fracturing, as shown in the schematic in Figure12(c). The mechanisms of graphene in toughening the copper matrix composites mainly included large interface strengthening, shear stress transfer strengthening, second-phase strengthening, and strengthening of the unique folded structure as the graphene exhibited good plasticity.

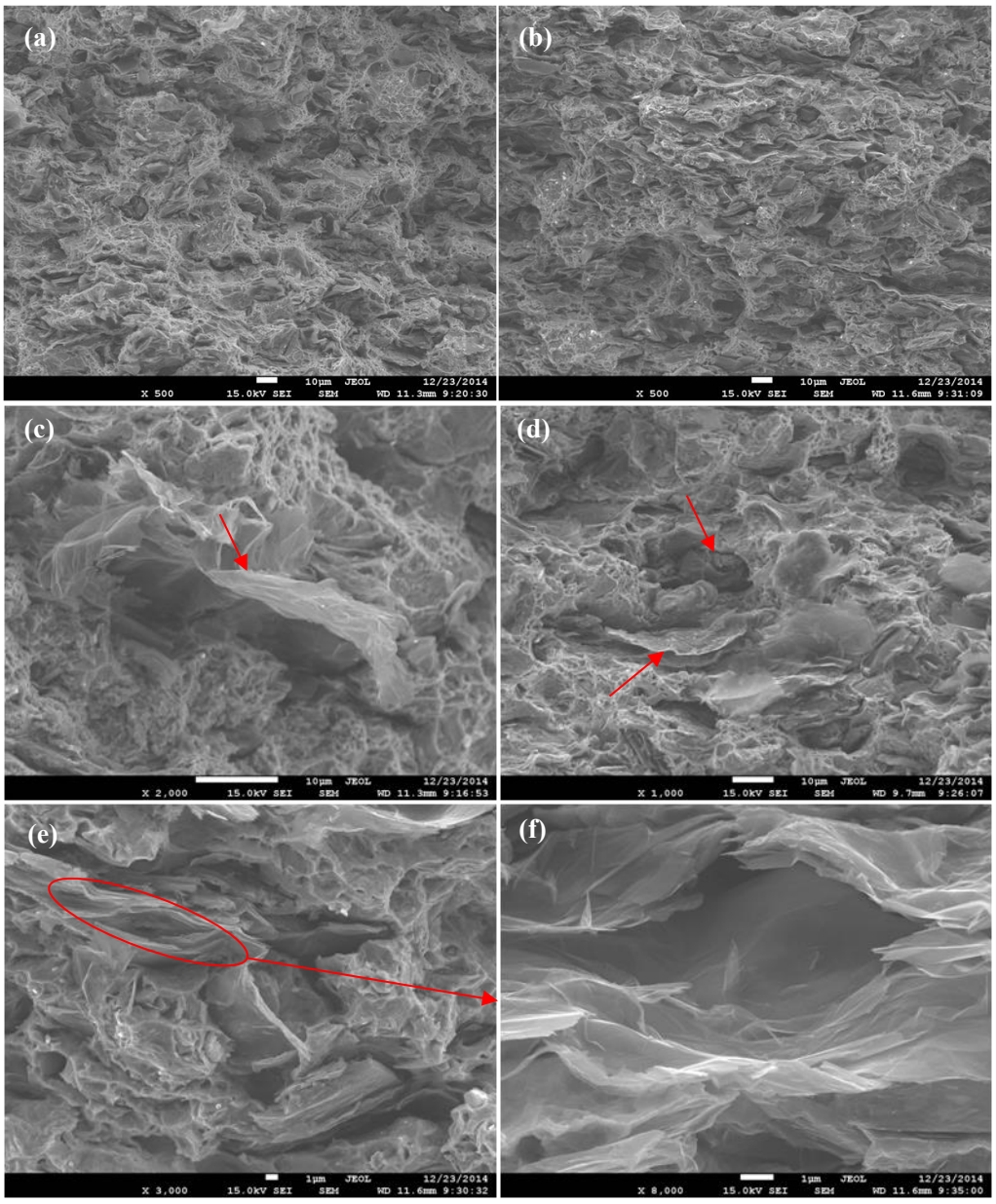

FIGURE 11 (a-b) SEM images of fractures of the sintered nanocomposites (0.5 wt.%, 1.5 wt.%). (c–e) SEM images of fractures of the sintered nanocomposites (0.5 wt.%, 1.0 wt.%, 1.5 wt.%). (f) Magnified SEM image of local amplification corresponding to Fig. 11(e).

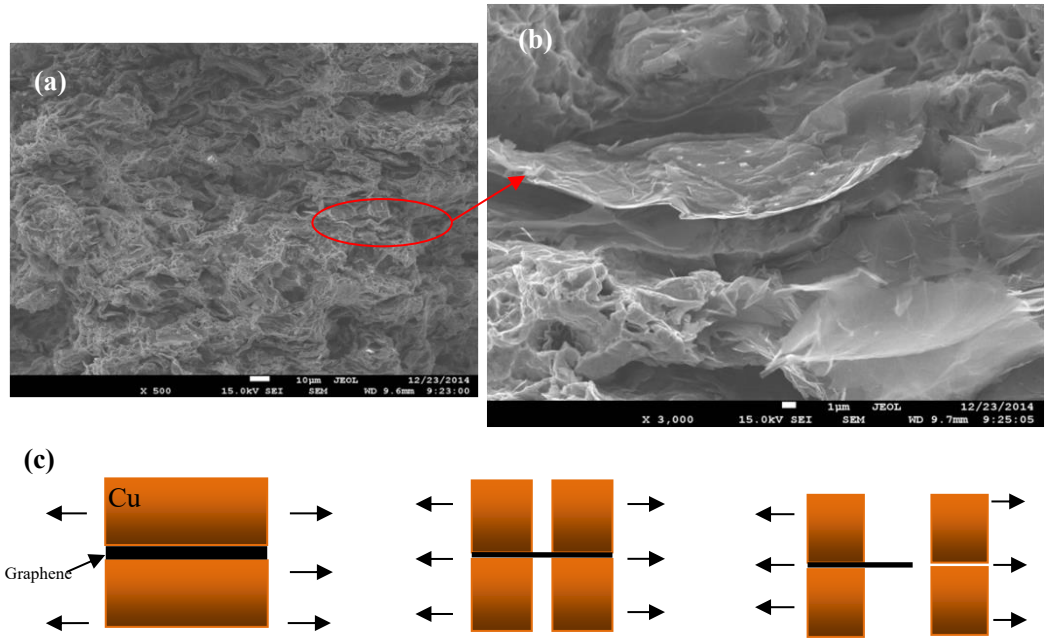

FIGURE 12:(a) SEM images of fractures of the nanocomposite with 1.0wt.% graphene. (b) Magnified SEM image of local amplification corresponding to Fig. 12(a). (c) Schematic diagram of tensile fracture microscopic process of graphene reinforced Cu matrix composites.

4. Conclusions

(1) Cu/Ti_3SiC_2/C/Graphene nanocomposites have been successfully fabricated by combined VHP and HIP. Addition of graphene can refine the microstructure because it can reduce nucleation energy and improve the nucleation rate. HIP not only provided further densification but also effectively eliminated the defects of the nanocomposites as the composite reached the highest compactness of 98.17% when graphene content was 0.5wt.%.

(2) Cu/Ti_3SiC_2/C/Graphene nanocomposites showed homogeneously dispersed graphene in the matrix with interface interaction products TiC and Cu_9Si generated by Ti_3SiC_2 thermal decomposition, resulting in highly enhanced mechanical properties. The micro Vickers hardness, tensile strength, compressive strength, and shear strength of the nanocomposites with 0.5wt.% graphene were129.17HV, 250.92 Mpa, 467.97 Mpa, and 129 Mpa, respectively, owing to the strengthening mechanisms of graphene.

(3) Observation of the tensile fractures of the Cu/Ti_3SiC_2/C/graphene nanocomposites, including the microporous aggregation fractures of the matrix, interfacial debonding fractures, transgranular fractures of the reinforcing particles, tears of the matrix, and cracks of the defects. In general, Ti_3SiC_2, C, and graphene were uniformly distributed in the Cu matrix, largely along the grain boundary. In this manner, dispersion-strengthening, dislocation strengthening, and graphene wrinkle effect can be the strengthening mechanisms.

Acknowledgements

This work was supported by National Natural Science Foundation of China (No. 51201143), China Postdoctoral Science Foundation (No. 2015M570794), Sichuan Science and Technology Support Program (No. 2016FZ0079), and R&D Projects Funding from the Research Council of Norway (No.263875/H30). The electron microscopy work at FSU was supported by the U.S. National Science Foundation No. 1436120. The TEM work was done at the Electron Microscopy Center at Argonne National Laboratory, which is operated by U Chicago Argonne, LLC, under Contract DE-AC02-06CH11357.

References

[1]G. Yu, X.H. Huang, C. Zou, C. Li, B.N. Hu, L. Y. Ye.
Preparation of graphite@Cu powders from ultrasonic powdering technique.
Adv Powder Technol, 23(1) 2012, pp. 16-21.
[2]C.P. Samal, J.S. Parihar, D.Chaira.
The effect of milling and sintering techniques on mechanical properties of Cu-graphite metal matrix composite prepared by powder metallurgy route.
J. Alloys Compd, (569)2013, pp. 95-101.
[3]Z. L. An, M. Toda, T. Ono.
Comparative investigation into surface charged multi-walled carbon nanotubes reinforced Cu nanocomposites for interconnect applications.
Compos Part B Eng, 95 (2016), pp. 137-143.
[4]D. Sarkar, B.V.M. Kumar, B. Basu.
Understanding the fretting wear of Ti_3SiC_2.
J Eur Ceram Soc, 26(13)2006, pp. 2441-2452.
[5]G. Górny, M. Rączka, L. Stobierski, K. Rożniatowski, P. Rutkowski.
Ceramic composite Ti_3SiC_2-TiB_2-Microstructure and mechanical properties.
Mater Charact, 60(10)2009, pp. 1168-1174.
[6]V. Pasumarthi, Y. Chen, S.R. Bakshi, A. Agarwal.
Reaction synthesis of Ti_3SiC_2 phase in plasma sprayed coating.
J. Alloys Compd, 484(1-2) 2009, pp. 113-117.
[7]A.K. Geim, K.S. Novoselov.
The rise of graphene.
Nat Mater, 6(3) 2007, pp. 183-191.
[8]C.G. Lee, X.D. Wei, W.K. Kysar, J. Hone.
Measurement of the elastic properties and intrinsic strength of monolayer graphene.
Science, 321(5887)2008, pp. 385-388.
[9]A.K. Geim.
Graphene: Status and prospects.
Science, 324(5934)2009, pp. 1530-1534.
[10]A. A. Balandin, S. Ghosh, W.Z. Bao, I. Calizo, D. Teweldebrhan, F. Miao, C.N. Lau.
Superior thermal conductivity of single-layer graphene.
Nano Letters, 8(3)2008, pp. 902-907.
[11]Y. W. Gao, P. Hao.
Mechanical properties of monolayer graphene under tensile and compressive loading.
Physica E Low-dimensional Systems and Nanostructures, 41(8)2009, pp. 1561-1566.
[12]S. K Georgantzinos., G. I. Giannopoulos, N. K. Anifantis.
Numerical investigation of elastic mechanical properties of graphene structures.
Mater Design, 31(10)2010, pp. 4646-4654.
[13]MarianaIoniţă, G. M. Vlăsceanu, A. A.a Watzlawek, S. I. Voicu, J. S. B. H. Iovu.
Graphene and functionalized graphene: Extraordinary prospects for nanobiocomposite materials.
Compos Part B Eng, 121 (2017), pp. 34-57.
[14]T.L. Ngai, W. Zheng, Y.Y. Li.

Effect of sintering temperature on the preparation of Cu-Ti_3SiC_2 metal matrix composite.
Prog Nat Sci-Mater, 23(1)2013, pp. 70-76.
[15]P. Sadowski , K. Kowalczyk-Gajewska, S. Stupkiewicz.
Classical estimates of the effective thermoelastic properties of copper–graphene composites.
Compos Part B: Eng, (80)2015, pp.278-290.
[16]X.S. Jiang,Liu, W.X. Li J.R., Z.Y. Shao, D.G. Zhu.
Microstructures and mechanical properties of Cu/Ti_3SiC_2/C/MWCNTs composites prepared by vacuum hot-pressing sintering.
J. Alloys Compd, (618) 2015, pp. 700-706.
[17] J.R. Li, X.S. Jiang, Z.Y. Shao, D.G. Zhu, S.S. Johnson, Z.P. Luo, M.H. Zhu.
Microstructure and Mechanical Properties of Multi-Phase Strengthened Al/Si/Al_2O_3/SiO_2/MWCNTs Nanocomposites Sintered by In Situ VacuumHot-Pressing.
J Nanomater, (10)2015, pp. 1-9.
[18]F.Sola, J. Niu, Z.H. Xia.
Heating induced microstructural changes in graphene/Cu nanocomposites.
J Phys D: Appl Phys, (46)2013, pp.1-7.
[19]J. Hwang, T. Yoon, S.H. Jin, J. Lee, T.S. Kim, S.H. Hong, S. Jeon.
Enhanced mechanical properties of graphene/copper nanocomposites using a molecular-level mixing process.
Adv Mater, (25)2013, pp. 6724-6729.
[20]Y. Kim, J. Lee, M.S. Yeom, J.W. Shin, H. Kim, Y. Cui, J.W. Kysar, J. Hone, Y. Jung, S. Jeon, S.M. Han.
Strengthening Effect of Single-atomic-Layer Graphene in Metal-Graphene Nanolayered Composites.
Nat Commun, (4) 2013, Article number: 2114.
[21]J. Shin, K. Choi, S. Shiko, H. Choi, D. Bae.
Mechanical damping behavior of Al/C60-fullerene composites with supersaturated Al–C phases.
Compos Part B Eng, 77 (2015), pp. 194-198.
[22]Z. Li, G. Fan, Q. Guo, Z. Li, Y. Su, D. Zhang.
Synergistic strengthening effect of graphene-carbon nanotube hybrid structure in aluminum matrix composites.
Carbon, (95)2015, pp. 419-427.
[23] L. Qu, L. Dai, E. Osawa.
Shape/size-controlled syntheses of metal nanoparticles for site-selective modification of carbon nanotubes.
J Am Chem Soc, 128(16) 2006, pp. 5523-5532.
[24]Kim, K.T.; Cha, S.I.; Hong, S.H.; Hong, S.H.
Microstructures and tensile behavior of carbon nanotube reinforced Cu matrix nanocomposites.
Mater. Sci. Eng. A., (430)2006, pp. 27-33.
[25]Zhang Bian-Xia,Yang Chun,Feng Yu-Fang, Yu Yi.
A density functional theory study of the absorption behavior of copper on single-walled carbon nanotubes.
Acta Phys. Sin., 58(6)2009, pp. 4066-4071.
[26]S .F. Bartolucci, J. Paras, M. A. Rafiee, J. Rafiee, S. Lee, D. Kapoor, N. Koratkar.
Graphene–aluminum nanocomposites.
Mater. Sci. Eng. A., 528(27)2011, pp. 7933-7937.

[27]M. Rashad, F. Pan, M. Asif, A. Tao.
Powder metallurgy of Mg–1%Al–1%Sn alloy reinforced with low content of graphene nanoplatelets (GNPs).
J Ind Eng Chem, 20(6)2014, pp. 4250–4255.
[28] S.E. Shin,Y.J. Ko, D.H. Bae.
Mechanical and thermal properties of nanocarbon-reinforced aluminum matrix composites at elevated temperatures.
Compos Part B Eng, 106 (2016), pp. 66-73.
[29]Z.R.Hu,G.Q.Tong,Q.Nian,R.Xu,M.Saei,F.Chen,CJ.Chen,M.Zhang,H.F.Guo,J.L.Xu.
Laser sintered single layer graphene oxide reinforced titanium matrix nanocomposites
Compos Part B Eng, 93 (2016), pp. 352-359.
[30]Z. Cao,X.D.Wang,J.L. Li,Y.Wu,H.P. Zhang,J.Q. Guo,S.Q. Wang.
Reinforcement with graphene nanoflakes in titanium matrix composites.
J. Alloys Compd, (696) 2017, pp. 498-502.
[31] Z. Xu, M. J. Buehler.
Interface structure and mechanics between graphene and metal substrates: A first-principles study.
J Phys-Condens Mat, 22(48)2010, Article number: 485301.
[32] G. I. Giannopoulos, I. G. Kallivokas.
Mechanical properties of graphene based nanocomposites incorporating a hybrid interphase.
Finite Elem Anal Des, 90(6)2014, pp. 31–40.
[33]W. H. Zhang, P. Wu, Z.Y. Li, J.L. Yang.
First-Principles Thermodynamics of Graphene Growth on Cu Surfaces.
Journal of Physical Chemistry C, 115(36)2011, pp. 17782-17787.
[34]X.Shi, Q. Yin, Y. Wei.
A theoretical analysis of the surface dependent binding, peeling and folding of graphene on single crystal copper.
Carbon, 50(8)2012,pp. 3055-3063.
[35]E. Jomehzadeh, N.M. Pugno.
Bending stiffening of graphene and other 2D materials via controlled rippling.
Compos Part B Eng, 83 (2015), pp.194-202.
[36]D. Bilgili, L. Kirkayak, M. Kirca.
The effects of intertube bridging through graphene nanoribbons on the mechanical properties of pillared graphene.
Compos Part B Eng, 120 (2017), pp. 1-9.
[37]H.G.P. Kumar, M.A. Xavior.
Graphene Reinforced Metal Matrix Composite (GRMMC): A Review.
Procedia Engineering, (97)2014, pp. 1033-1040.
[38]D. D. Kulkarni, I. Choi, S. S. Singamaneni, V.V. Tsukruk.
Graphene oxide-polyelectrolyte nanomembranes.
Acs Nano, 4(8)2010, Article number: 4667.
[39]J.Y. Suh,D. H. Bae.
Mechanical properties of polytetra fluoroethylene composites reinforced with graphene nanoplatelets by solid-state processing.
Compos Part B Eng, 95 (2016), pp. 317-323.

[40]S. Gupta, B.McDonald, S.B.Carrizosa, C.Price.
Microstructure, residual stress, and intermolecular force distribution maps of graphene/polymer hybrid composites: Nanoscale morphology-promoted synergistic effects.
Compos Part B Eng, 92 (2016), pp. 175-192.
[41]M.W. Lee, T.Y. Wang, J.L.Tsai.
Characterizing the interfacial shear strength of graphite/epoxy composites containing functionalized graphene.
Compos Part B Eng, 98 (2016), pp. 308-313.
[42]A. Genoese, A. Genoese, N. L. Rizzi, G. Salerno.
On the derivation of the elastic properties of lattice nanostructures: The case of graphene sheets.
Compos Part B Eng, 115 (2017), pp. 316-329.
[43]Y.T. Peng, Y.R. Hu, L.Z. Han, C.X. Ren.
Ultrasound-assisted fabrication of dispersed two-dimensional copper/reduced graphene oxide nanosheets nanocomposites.
Compos Part B Eng, 58 (2014), pp. 473-477.
[44]L.H. Fu,W. Han, K. Gong, S. Bengtsson, C.F. Dong, . Zhao, Z.L. Tian.
Microstructure and tribological properties of Cr_3C_2/Ni_3Al composite materials prepared by hot isostatic pressing (HIP).
Mater Design, 115(5)2017, pp. 203-212.
[45]X.S. Jiang, Z.Y. Shao, J.R. Li, W.X Liu., D.G. Zhu, D. Liu..
Dispersion Characteristics of Multi-Walled Carbon Nanotubes with Gallic Acid.
J Nanosci Nanotechno, (15)2015, pp. 9874-9878.
[46]J.R. Li, X.S. Jiang, R. Shen, Z.Y. Shao, D.G. Zhu, D. Liu..
Dispersion Characteristics of Multi-Walled Carbon Nanotubes and Carbon Nanoflakes with Oxygen Plasma.
Nanosci Nanotech Let, (7)2015, pp. 581-587.
[47]M. Bastwros, G.Y. Kim, C. Zhu, K. Zhang, S.Wang, X.Tang, X. Wang.
Effect of ball milling on graphene reinforced Al6061 composite fabricated by semi-solid sintering.
Compos Part B Eng, 60 (2014), pp. 111-118.
[48]H. J. Choi, J. H. Shin, D. H.Bae.
The effect of milling conditions on microstructures and mechanical properties of Al/MWCNT composites
Compos Part A Appl S, 43(7) (2012), pp.1061-1072.
[49]Y. Tang, X. Yang, R. Wang, M. Li.
Enhancement of the mechanical properties of graphene-copper composites with graphene-nickel hybrids.
Mat Sci Eng A-Struct, (599)2014, pp. 247-254.
[50]K. Shirvanimoghaddam, S. U. Hamim, M.K. Akbari, S. M. Fakhrhoseini, H.Khayyam, A. H. Pakseresht, E. Ghasali, M. Zabet, K. S. Munir, S.Jia, J. P.Davim, M. Naebe
Carbon fiber reinforced metal matrix composites: Fabrication processes and properties.
Compos Part A Appl S, 92 (2017), pp.70-96.
[51]J.R. Lu, Y. Zhou, H.Y. Li, Y. Zheng, S.B. Li, Z.Y. Huang.
Wettability and Wetting Process in Cu/Ti_3SiC_2 System.
J Inorg Mater, 29(12)2014, pp. 1313-1319.
[52]S. Basavarajappa, G. Chandramohan, J.P. Davim.

Application of Taguchi techniques to study dry sliding wear behaviour of metal matrix composites.
Mater Design, 28(4)2007, pp. 1393–1398.
[53]P.J.Bin, W.L.Ping, X.Q Ji.
Progress of Tribology of Graphene and Graphene-based Composite Lubricating Materials.
Tribology, (34)2014, pp. 93-112.
[54]A. D. Moghadam, E. Omrani, P. L. Menezes, P. K. Rohatgi.
Mechanical and tribological properties of self-lubricating metal matrix nanocomposites reinforced by carbon nanotubes (CNTs) and graphene – A review.
Compos Part B Eng, 77 (2015), pp. 402-420.
[55]A.El-Ghazaly, G. Anis, H. G. Salem.
Effect of graphene addition on the mechanical and tribological behavior of nanostructured AA2124 self-lubricating metal matrix composite.
Compos Part A Appl S, 95 (2017), pp.325-336.
[56]C.L.P. Pavithra, B.V. Sarada, K.V. Rajulapati, T.N. Rao, G.A. Sundararajan.
New Electrochemical Approach for the Synthesis of Copper-Graphene Nanocomposite Foils with High Hardness.
Sci Rep-Uk 4(6)2014, Article number: 4049.
[57]Rashad, M.; Pan, F. S.; Asif, M. Exploring mechanical behavior of Mg-6Zn alloy reinforced with graphene nanoplatelets.
Mater. Sci. Eng. A., (649)2016, pp. 263-269.
[58]W.X. Liu, X.S. Jiang,Z.Y. Shao,D.F. Mo,D.G. Zhu,M. Zhang. Tribological behaviors of $Cu/Ti_3SiC_2/C/MWCNTs$ composites with electric current.
J ComputTheor Nanos. 12(9)2015, pp. 2664-2672.
[59]M. Rashad, F.S. Pan, A.T. Tang, M. Asif.
Effect of Graphene Nanoplatelets addition on mechanical properties of pure aluminum using a semi-powder method.
Prog Nat Sci-Mater, 24(2)2014, pp.101-108.
[60]M. Rashad, F.Pan, A. Tang, M. Asif, J. She, J.Gou, J. Mao, H. Hu.
Development of magnesium-graphene nanoplatelets composite.
J. Compos. Mater., (49)2015, pp.285-293.
[61]R. Jiang, X. Zhou, Q. Fang.
Copper–graphene bulk composites with homogeneous graphene dispersion and enhanced mechanical properties.
Mater. Sci. Eng. A., (654)2016, pp. 124-130.
[62]J.Y. Wang, Z.Q. Li, G.L. Fan, H.H. Pan, Z.X. Chen, D. Zhang.
Reinforcement with graphene nanosheets in aluminum matrix composites.
Scripta Mater, 66(8)2012, pp. 594–597.
[63]S.L. Xiang, M. Gupta, X.J. Wang, L.D. Wang, X.S. Hu, K. Wu.
Enhanced overall strength and ductility of magnesium matrix composites by low content of graphene nanoplatelets.
Compos Part A Appl S, 100 (2017), pp.183-193.
[64]Z.P. Luo.
Statistical quantification of the microstructural homogeneity of size and orientation distributions.
J Mater Sci, (45)2010, pp. 3228-3241.

[65]W.X. Liu, X.S. Jiang, Z.Y. Shao, D.G. Zhu, M.H. Zhu, S. S. Johnson, Z.P. Luo.
Nanocarbon-reinforced Cu-matrix nanocomposites with high High Mechanical Strengths.
Curr Nanosci, 13(4)2017, pp. 410-420.
[66]C. Zhao, J. Wang.
Fabrication and tensile properties of graphene/copper composites prepared by electroless plating for structural applications.
Phys Status Solidi A, 12(211)2014, pp. 2878-2885.
[67]S.E. Shin, D.H. Bae.
Deformation behavior of aluminum alloy matrix composites reinforced with few-layer graphene.
Compos Part A Appl S, 78 (2015), pp.42-47.